Catalysis Letters (2018) 148:2561–2571
https://doi.org/10.1007/s10562-018-2435-z

Novel Synthesis of Cu@ZnO and Ag@ZnO Nanocomposite via Green Method: A Comparative Study for Ultra-Rapid Catalytic and Recyclable Effects

G. Manjari[1] · S. Saran[1] · Suja P. Devipriya[1] · A. Vijaya Bhaskara Rao[1]

Received: 5 February 2018 / Accepted: 28 May 2018 / Published online: 5 June 2018

Abstract

The use of metal immobilized/decorated nanocomposites as catalyst were usually used in environmental pollution remediation and protection, industrial production, and biomedical applications. Finding a new and efficient method for the green synthesis of metal nanoparticles immobilized over porous material is of great interest. Synthesis of more stable and outstanding Cu@ZnO and Ag@ZnO nanocomposite for nitro aromatic compound reduction were reported in this work. The metal nanoparticles and nanocomposite was characterized using UV–Vis spectrum, XRD, Raman spectra, TEM, SAED, EDS, and FTIR techniques. The immobilized Cu and Ag nanoparticles are with an average size of 18 and 12 nm on ZnO surface respectively. Comparatively, the Cu/ZnO and Ag/ZnO nanocomposite acted as an efficient heterostructure catalyst in the reduction of p-nitrophenol to p-aminophenol than pure Cu and Ag nanoparticles with more stability up to six cycles. The characterization results inferred the synergic effect between metal and porous material played important role in its activity and stability of Cu@ZnO and Ag@ZnO nanocomposite more than pure Cu and Ag nanoparticles. It is proposed that Cu and Ag immobilized ZnO applicable in various catalytic activities were achieved.

Graphical Abstract

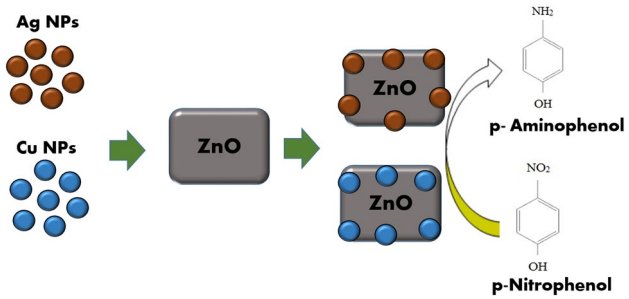

Keywords Green synthesis · *Aglaia elaeagnoidea* · Ag@ZnO, and Cu@ZnO nanocomposites · p-Nitrophenol · Homogenous and heterogeneous catalysis

1 Introduction

The fascination of nanomaterials emanated from the inherent properties, they evinced the significant difference as of their bulk counterparts [1, 2]. The metal nanoparticles are gaining more attention due to their surface plasmonic properties that shown promise application in catalysis, sensing, photocatalysis, biomedical, and drug delivery [3–6]. Metallic

✉ G. Manjari
gangarapumanjari@gmail.com

[1] Department of Ecology and Environmental Sciences, Pondicherry University, Puducherry 605014, India

nanoparticles efficiency depended on its size, morphology, crystalline nature, and composition. Developments in the designing and synthesis of nanomaterials with control size at atomic level might be offering enhanced opportunities as heterogeneous nanocatalyst [7]. The catalytic activity of individual nanoparticles is limited due to their leaching and its aggregation [8]. The heterogeneous catalytic efficiency of nanomaterials either in isolated form or as nanocomposite in various applications was studied [7]. Combination of more than one nanomaterials have exhibited greater applications, due to the coupling between isolated nanomaterial properties [9].

Nowadays, different combination nanomaterials such as Co_2P/ZnO@PC/CNTs as bimetal nanomaterials, Pd@Pt/rGO, Ni doped Ag@C as core shell nanomaterials, Cu and silver/polymer as polymer nanocomposite and metal/porous oxide these might be used by coating/surface modification nanocomposites attracting more for its activity and stability to make them reconcilable for chosen applications [10–14]. These nanocomposites not only attained enhanced activity but also stable at high temperature and pressure [15]. Among the vast possibilities, synthesis and application of metal/metal oxide nanocomposite have been gaining significant attention and contributing itself an immense of advanced nanomaterials chemistry [12]. For immobilization of metal nanoparticles, oxides such as ZnO, TiO_2, MgO, GO, and $FeSO_4$ acts an excellent support [16–20].

The semiconductor ZnO is an inorganic compound and it has numerous favorable properties such as wide band gap, high electron transport, and good transparency and has been widely used in various fields [21]. It was used as a porous support material for metal nanocatalyst, due to its chemical and thermal stability [22]. Immobilization of less expensive metal nanoparticles such as Ag, Cu and Ni, on support material ZnO surface to improve the catalytic activity due to the unexpected interplay of lattice and electron effects in adjacent metals [23]. However, the manuscript obtained an advantage of synthesis of Ag and Cu NPs using plant extract and immobilized over the surface of zinc oxide (ZnO). Therefore, green synthesis of nanocomposite was gaining much attention in recent years, due to its ease, compatibility, low cost, safe, and sustainable with biomedical, environmental, sensing, drug delivery and drug manufacturing applications is the advantages of green synthesis over other synthesis methods.

Aglaia elaeagnoidea (A. Juss) (syn. *A. roxburghiana*) is an every green tree belongs to the Meliaceae family and distributed in the tropical forests of Asia and usually found in coast regions [24]. The plant was used in the treatment of antidiarrhoeal, anti-inflammatory, and also used to treat tumors and skin diseases [25]. *Aglaia elaeagnoidea* bark aqueous extract shown the presence of high amount of phenolic compounds and other phytochemicals and also exhibited high antioxidant activity [26]. Herein, we successfully synthesized Ag and Cu nanoparticles and immobilized over ZnO surface as nanocomposite using *A. elaeagnoidea* bark extract, a greener method. We have compared, the efficacy of homogenous, pure and immobilized heterogeneous activity of Ag and Cu nanoparticles on the reduction of p-nitrophenol (p-NP) to p-Aminophenol (p-AP) at room temperature.

2 Materials and Methods

2.1 Materials

Zinc Oxide (ZnO, Commercial grade) with specific surface of 17.2 m^2/g was selected as support material, metal precursors like copper nitrate ($Cu(NO_3)_2 \cdot 3H_2O$), and silver nitrate ($AgNO_3$), and p-NP were purchased from Himedia Laboratories Ltd. India. Methyl orange, rhodomine blue, and sodium borohydride were purchased from Sigma-Aldrich.

2.2 Preparation of Extract

Aglaia elaeagnoidea bark was collected and shade dried for seven days, grind into fine powder. Take 250 ml conical flask with 10 g of bark material and 130 ml of deionised water were added and then, refluxed for 10 min on a magnetic stirrer. The bark extract was centrifuged for 10 min to remove plant debris at 6000 rpm and filtered through Whatman filter paper.

2.3 Green Synthesis of Cu and Ag Nanoparticles

For the preparation of Cu and Ag nanoparticles, 10 ml of *A. elaeagnoidea* aqueous bark was added to 90 ml of 1 mM Cu and Ag precursor solution at the room temperature. The immediate color change was observed, that indicates the synthesis of Cu and Ag NPs.

2.4 Immobilization of Green Synthesized of Cu@ZnO and Ag@ZnO

The metal support ZnO was prepared by dispersing of 1 g of ZnO in 100 ml of Cu NPs were sonicated for 30 min for uniform dispersion. The same procedure was followed for the Ag/ZnO nanocomposite. For moisture evaporation from both metal nanocomposite mixtures, shifted to a hot air oven for 6 h at 140 °C and organic matter was removed by calcination at 400 °C. The final loading of the metal nanoparticles on ZnO surface is about 7.1 and 9.9 mg respectively for Cu and Ag NPs, which was analyzed through ICP-AES by digesting the samples in the acid.

2.5 Characterization Methods

The prepared metal nanoparticles/nanocomposites were confirmed using following analysis, UV–Vis–NIR Spectrophotometer (Make: Varian Model: 5000) for optical properties change. X-ray diffraction (XRD, Philips PW 3710/3020) measurements for crystalline nature of Cu and Ag NPs, Cu@ZnO and Ag@ZnO nanocomposite. The stretching vibration of prepared nanocomposite were determined by Raman spectrometer. Morphology of Cu and Ag NPs, Cu@ZnO and Ag@ZnO nanocomposite was confirmed by transmission electron microscopy (TEM, JEOL; model 2010). Energy Dispersive X-ray Spectroscopy (EDAX, S3700N) were performed for the chemical composition of synthesized nanocomposites. The role of phytochemicals of extract in the synthesis of metal nanoparticles was confirmed by Fourier transform infrared (FTIR, Nicolet; model 6700) spectrophotometer of the range of 400–4000 cm^{-1}. The leaching of metal content after catalytic activity in nanocomposite was evaluated by an Inductively Coupled Plasma-Atomic Emission Spectrometer (ICPAES, Model: Jobin Yvon Horiba).

2.6 Catalytic Performance

2.6.1 Homogenous Activity of Cu and Ag NPs

The catalytic performance of green synthesized of Cu and Ag NPs were tested, 100 µl of a liquid solution of nanoparticles has taken as an optimum concentration. And 1 ml of 10^{-3} M p-NP were added to 1 ml of 10^{-2} M sodium borohydride ($NaBH_4$) solution as reducing agent, then 100 µl of metal catalyst were added and the reaction was monitored using UV–Vis spec.

2.6.2 Heterogeneous Activity of Pure Cu and Ag NPs

For the catalytic efficiency of Cu and Ag NPs, an equal proportion (1 ml) of 10^{-3} M p-NP, with 10^{-2} M $NaBH_4$ in the presence of 5 mg of prepared nanomaterials was evaluated as a model reaction. In the end of the catalytic reaction, nanomaterials were recovered by centrifugation and reused.

2.6.3 Heterogeneous Activity of Cu@ZnO and Ag@ZnO Nanocomposite

Reduction of p-NP was investigated in 2 ml micro centrifuge tube in the presence of Cu@ZnO and Ag@ZnO nanocomposite with $NaBH_4$ at room temperature. The liquid phase of 1 ml of 10^{-3} M p-NP was mixed with 10^{-2} $NaBH_4$. To the mixture, 4 mg of Cu/ZnO nanocomposite was added. The catalytic efficacy of Ag/ZnO nanocomposite was tested using the same procedure. The nanocomposite was separated using centrifugation for next successive cycles.

3 Results and Discussion

3.1 Characterization of Cu and Ag NPs on ZnO

3.1.1 Optical Properties

The reduction of copper and silver metal precursors to Cu and Ag NPs in aqueous solution were confirmed by UV–Vis spectra, the immediate color change of mixture after addition of bark extract was observed. Due to the surface plasmon vibrations (SPR), the color of the mixture was changed from light brownish to brick red for Cu NPs (Fig. 1) and dark brownish for Ag NPs (Fig. 1). The UV–Vis–NIR spectrophotometer optical absorbance of immobilization of Cu and Ag NPs on a surface of ZnO were investigated. As noticed in Fig. 2 absorption peak of pure ZnO at 365 nm attributed to the excitonic absorption of ZnO [27]. For Cu/ZnO nanocomposite the intensity of absorption peak is lower in the ultraviolet region. But it is slightly shift and broaded in the visible region for both Cu@ZnO and Ag@ZnO nanocomposite while compared to the ZnO [28, 29]. The interfacial coupling among Ag NPs and ZnO might be a reason for the shift of plasmon absorption of Ag@ZnO. The metal nanoparticles SPR was depends on metal an electron density [10]. The absorption peak of green synthesized Cu and Ag NPs are quite stable even for 3 months that might be due to various phytochemicals of bark extract.

3.1.2 Structural Properties

The crystallographic and phase structure of green synthesized Cu and Ag NPs immobilized on ZnO were compared

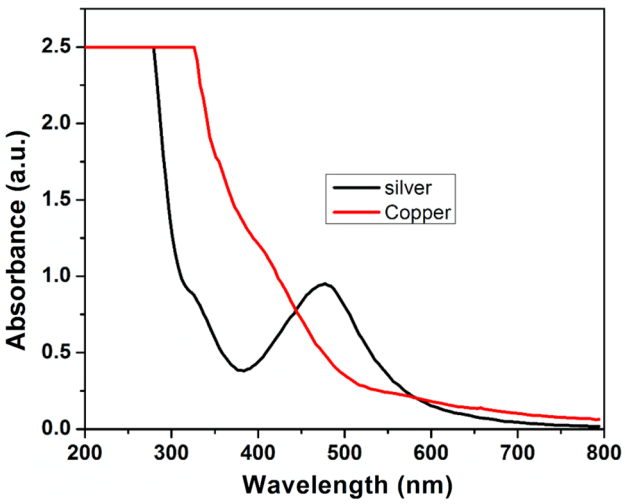

Fig. 1 UV–Visible spectra of liquid Ag, Cu and Ag–Cu alloy nanoparticles

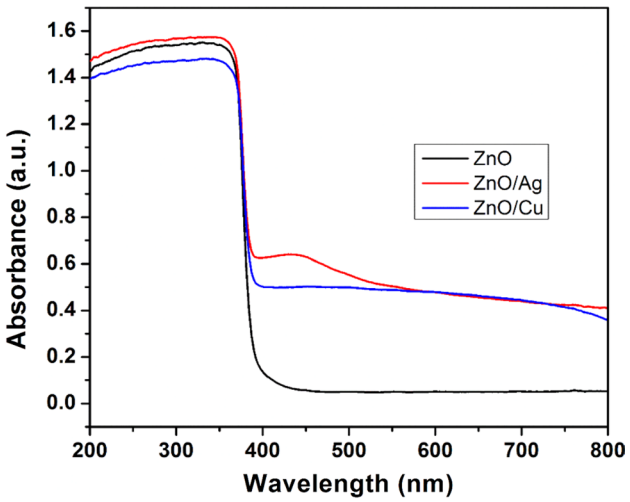

Fig. 2 UV–Visible spectra of Ag/ZnO and Cu/ZnO nanocomposite

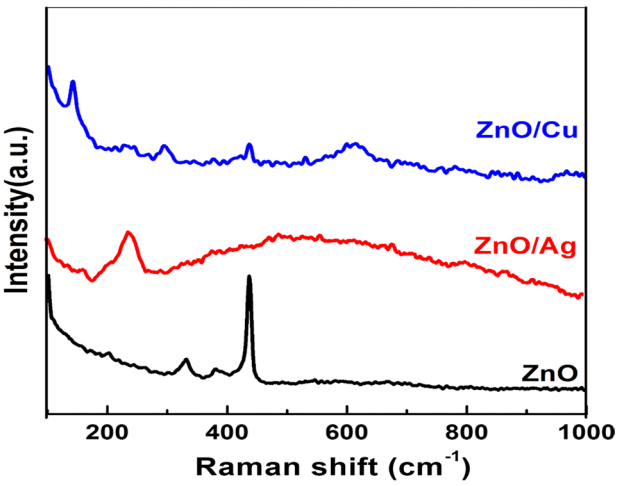

Fig. 4 Raman spectra of ZnO, Ag/ZnO, and Cu/ZnO nanocomposite

with pure ZnO using XRD analysis (Fig. 3). The Cu and Ag NPs support on ZnO nanocomposite exhibited exactly same series of characteristic peaks as that of wurtzite hexagonal phase peaks of pure ZnO i.e., 31.78°, 34.42°, 36.28°, 47.56°, 56.62°, 62.86°, 67.96° and 69.10° (JCPDS card no. 089-0511). There is no significant difference were observed between Cu@ZnO, Ag@ZnO and ZnO diffraction patterns which might be due to very low concentration of metal nanoparticles immobilized over ZnO and deposition of metal atoms near the surface of ZnO [16, 30].

The Raman spectra for pure ZnO and Cu and Ag immobilized nanocomposites are shown in Fig. 4 with backscattering ranging from 200 to 1000 cm. The centre optical phonon of wurtzite hexagonal type ZnO belongs to the C_{6v} space group i.e., $A_1 + 2B_1 + E_1(x, y) + 2E_2$ [31]. The polar modes A_1 and E_1 are split into two frequencies such as transverse optical (TO) and longitudinal optical (LO) phonon component modes. The B_1 phonon modes are Raman silent or

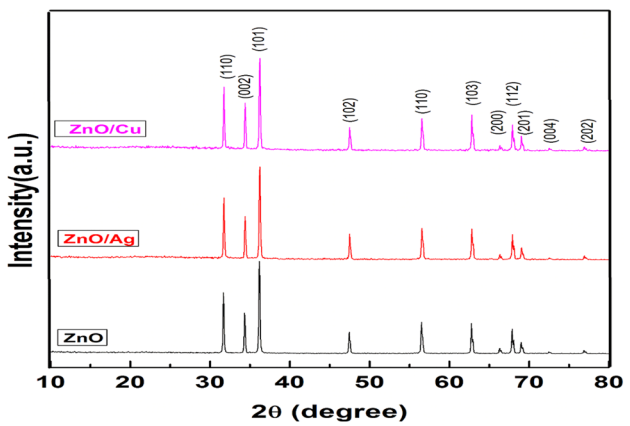

Fig. 3 XRD pattern of ZnO, Ag/ZnO, and Cu/ZnO nanocomposite

inactive whereas The E_2 modes are Raman active non-polar with two frequencies [32]. In E_2(high) only oxygen atoms are associated and it is characteristic feature of wurtzite phase, and the E_2(low) mode in ZnO related with Zn sublattice [31]. The peak at 437 cm^{-1} of pure ZnO correspond to E_2(high) and other peaks around 330 cm^{-1} might be attributed to E_2(high)–E_2(low) modes due to multi-phonon development. The Raman peak at 383 cm^{-1} assigned to A_1 (TO) [33]. Both E_2(high) and E_2(low) modes are observed in Cu/ZnO while in Ag/ZnO only E_2(low) mode is present. The Raman band intensity of modes are reduced in both Cu and Ag immobilized ZnO and slightly red-shift in E_2(high) and E_2(low) modes also observed. The results indicate red-shift in E_2(high) and E_2(low) modes leads to change in the structure of ZnO by incorporation of Cu and Ag nanoparticles into the lattice sites of Zn^{2+} [34].

3.1.3 Morphological Properties

The morphological properties of Cu and Ag nanoparticles immobilized over ZnO were investigated by TEM. The green synthesized Cu NPs on ZnO surface are spherical in shape with an average size of 18 nm (Fig. 5a, b). Ag NPs anchored on ZnO are spherical with 12 nm (Fig. 6a, b). The crystalline nature of Cu and Ag NPs on ZnO were shown in SAED patterns (Figs. 5c, 6c). Figure 7a, b depicts the EDS, which reveals the presence of metal in nanocomposite, that indicating the reduction of elemental silver and copper ions into nanoparticles.

3.1.4 FTIR Analysis

Figure 8 shown FTIR measurements of the aqueous extract and Cu and Ag NPs and it confirms the phytochemicals of *A. elaeagnoidea* bark plays a crucial role in

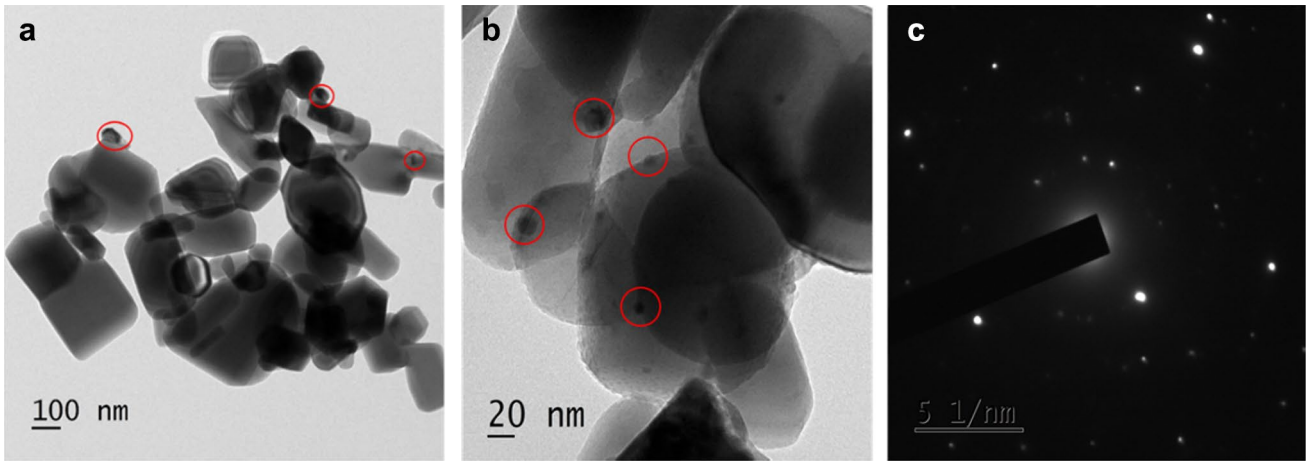

Fig. 5 TEM image of Cu/ZnO (**a**), **b** red circle focused on Cu NPs and **c** SADE of Cu/ZnO nanocomposite

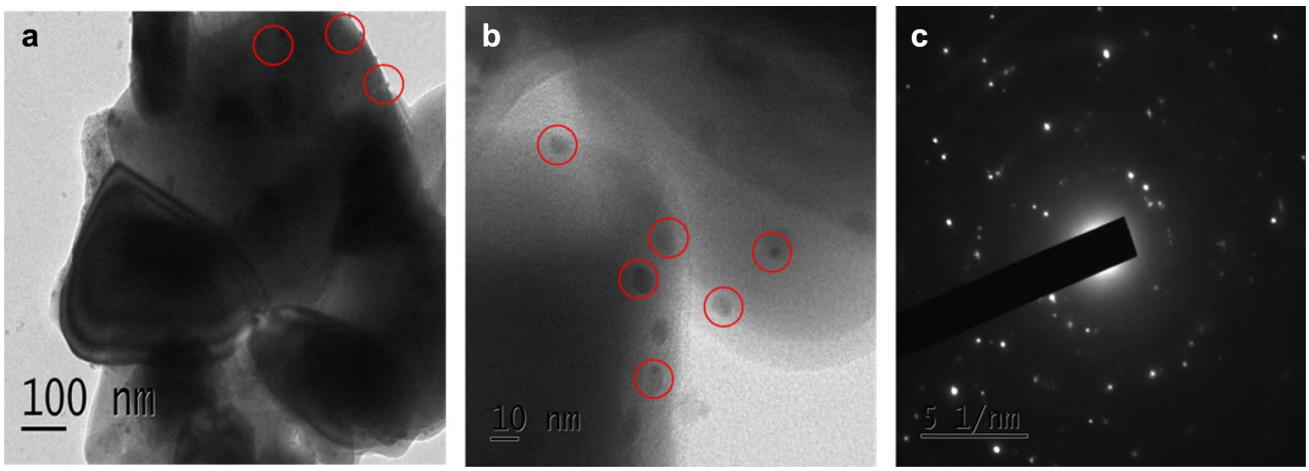

Fig. 6 TEM image of Ag/ZnO (**a**), **b** red circle focused on Ag NPs and **c** SADE of Ag/ZnO nanocomposite

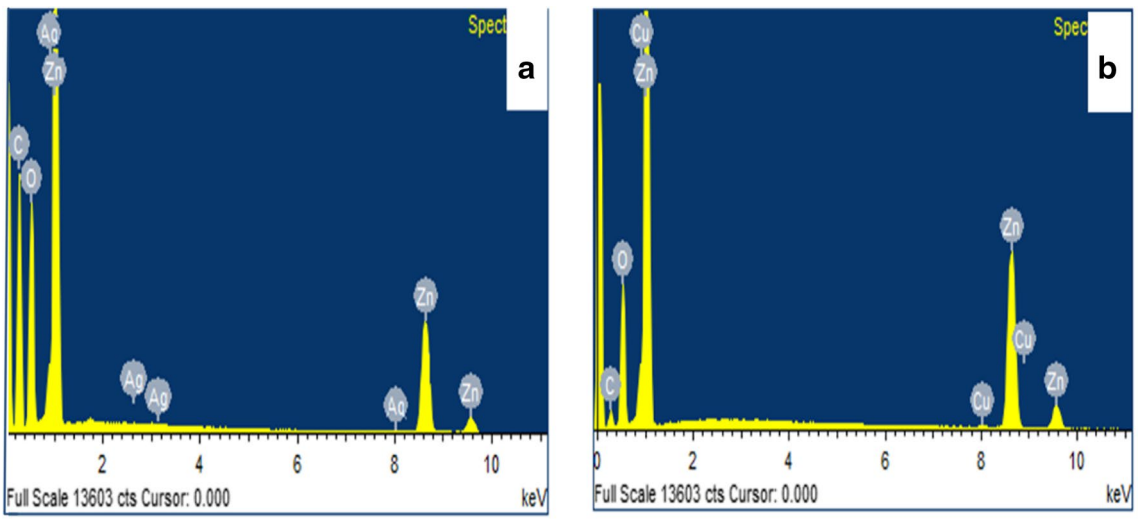

Fig. 7 EDS image of **a** Cu/ZnO and **b** Ag/ZnO nanocomposite

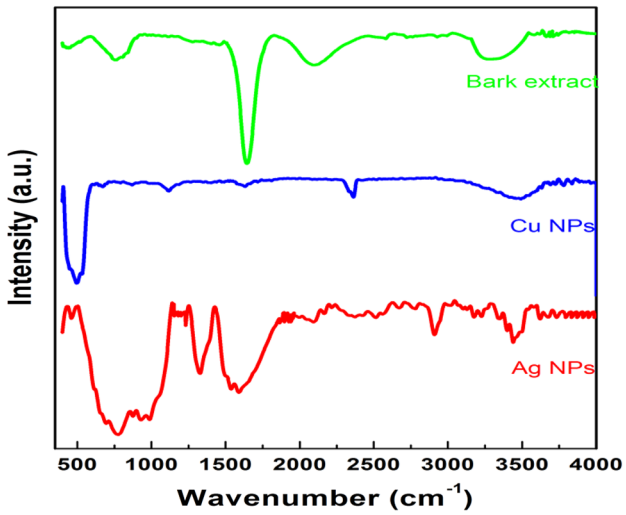

Fig. 8 FTIR spectra of *A. elaeagnoidea* bark extract, Cu and Ag NPs

the production of Cu and Ag NPs. The intensity band in the IR spectra of the extract comprises of notable peaks at 3279, 2993, 1643, and 763 respectively corresponds to alcoholic/phenolic O–H stretch, alkane C–H stretching, the primary and secondary amines along with amide linkage of proteins/enzymes and aromatic C–H bending [35, 36]. All the peaks of extract are shifted and reduced in the synthesis of Cu and the peaks are weakening in Ag NPs. The presence of phytochemicals such as phenolic compounds, proteins, alkaloids, and other phytochemicals are responsible for the reduction and capping agent.

3.2 Catalytic Activity of Nanocomposite

p-NP are used as intermediate for the production p-AP (4-aminophenol). Synthesis of p-AP is commercially important, due to its demand as intermediate in the drug manufacturing industry, especially in antipyretic and analgesic and also used in dye industries, enormously as a photo film developer, and anticorrosion-lubricant etc. [37]. Synthesis of p-AP by conventional methods through stoichiometric quantities of iron/hydrochloric acid as reducing reagents were with some limitations [38]. Hence, nanotechnology established as new alternative method in eco-friendly manner.

3.2.1 Homogenous Catalytic Activity of Cu and Ag NPs

The homogenous catalytic activity of green synthesized Cu and AgNPs (100 µl/ml) for reduction of p-NP in the presence of $NaBH_4$ in equal proportion has been investigated. All the sites of the catalyst are actively accessible for the reactants and exhibited great catalytic activity [39]. Addition of $NaBH_4$ as reducing agent to the p-NP, a shift of peak from 317 to 400 nm was observed which was due to the formation of phenolate ion [40]. When the Cu and Ag NPs (100 µl/ml) were added to the solution, change in solution color from pale yellow to colorless were observed with formation of a new absorption peak at 300 nm indicate reduction of p-NP to p-AP (Figs. 9a, 10a) [41]. The surface of the catalyst (Cu and Ag NPs) serves as an electron transfer among oxidizing and reducing agent (p-NP and $NaBH_4$). The reactants concentration remained constant, the rate constant for the p-NP reduction were demonstrated using pseudo-first-order kinetics [37].

$$-\mathrm{In}(Ct/C0) = \mathrm{In}(At/A0) = kt \quad (1)$$

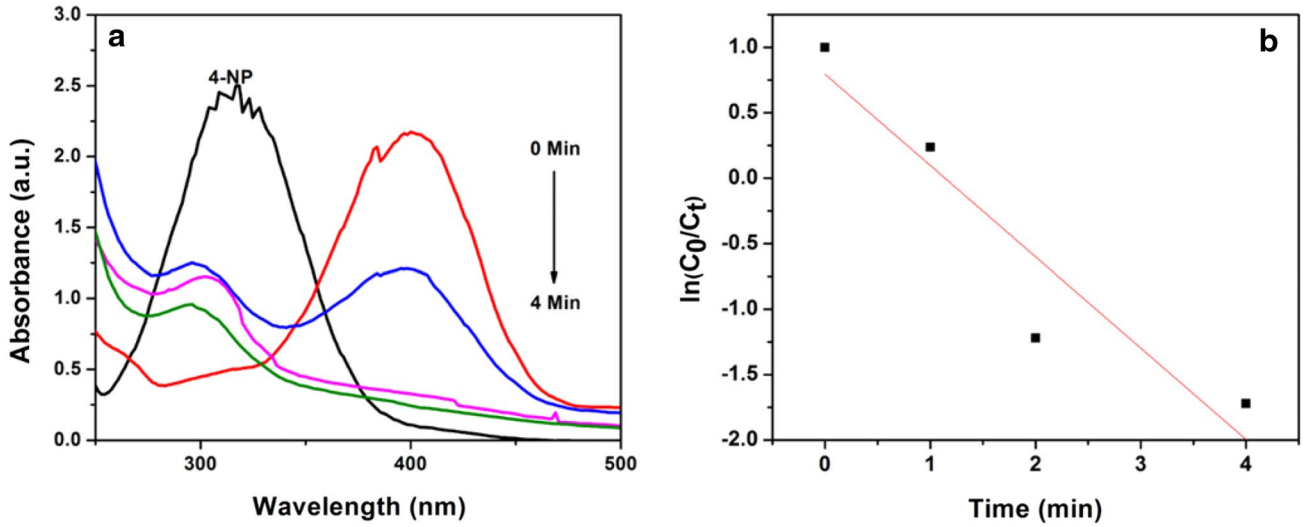

Fig. 9 UV–Vis spectra of homogeneous reduction of 4-NP **a** before and after addtion of $NaBH_4$ and Cu NPs liquid and **b** rate constant

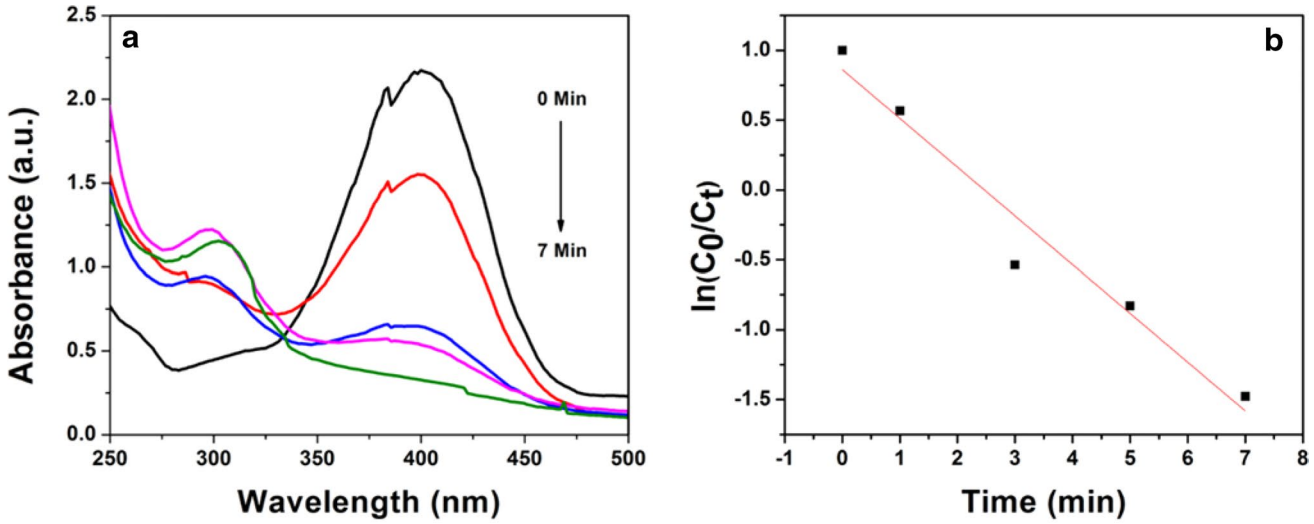

Fig. 10 UV–Vis spectra of homogeneous reduction of 4-NP **a** after addition of $NaBH_4$ and Ag NPs liquid and **b** rate constant

where k is the rate constant at the given time and t is the reaction time. C_0 and C_t concentrations of p-NP at initial and at time t respectively. The linear correlation among In(Ct/C0) and the reaction time for p-NP reduction was shown in Figs. 9b, and 10b and the rate constant for CuNPs and AgNPs was calculated as 0.6978 and 0.3482 min^{-1} respectively [42].

3.2.2 Heterogeneous Catalytic Activity of Cu and Ag NPs

Reuse and recyclability is major drawbacks in homogenous catalytic activity. In heterogeneous method, catalytic reaction between different phases i.e., solid metal nanoparticles and liquid phase dye solutions were used to overcome this drawbacks [43]. The catalytic efficacy of Cu and Ag NPs were proven through the reduction of 10^{-3} M p-NP, in the presence of reducing agent were decisively demonstrated using a UV–Vis spectra (Fig. 11a, b). The red shift in the absorption peak of p-nitrophenolate ion at 316–300 nm with very short time, indicate p-NP reduction. The catalytic reaction of Cu and Ag NPs for reduction of p-NP was completed in few seconds (45 and 72 s), the UV–Vis spectra was declined.

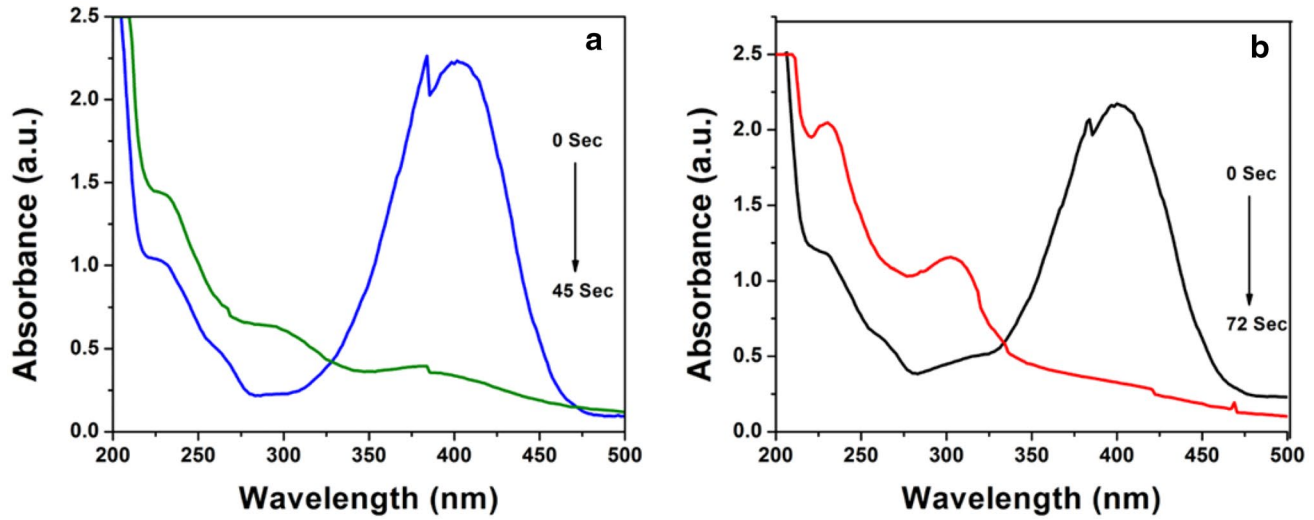

Fig. 11 UV–Vis spectra of heterogeneous reduction of 4-NP **a** pure Cu NPs and **b** pure Ag NPs

3.2.3 Heterogeneous Activity of Cu/ZnO and Ag/ZnO Nanocomposite

In heterogeneous catalytic activity of pure Cu and Ag NPs, leaching of metal nanoparticles in the reaction phase, that might be leads to lower reusability and recyclability [42]. Figure 12a, b shows the catalytic activity of Cu/ZnO and Ag/ZnO nanocomposite for the formation p-AP. After adding of nanocomposite to the p-NP and $NaBH_4$ mixture, instant color change was observed and the peak intensity was decreased with simultaneous raise of new peak at 295 nm within few seconds, corresponds to p-AP. In control, the reduction of p-NP by $NaBH_4$ reaction not completed up to 24 h without catalyst due to large kinetic barrier among 4-NP and $NaBH_4$ [44]. Therefore, the superior catalytic efficiency of Cu@ZnO and Ag@ZnO nanocomposite were attained. Cu@ZnO nanocomposite exhibited enhanced catalytic efficiency than Ag/ZnO nanocomposite. The catalytic reaction completed in very short time so the UV–Vis absorption spectra declined.

Scheme 1 depicts the possible mechanism for the reduction of 4-NP in the presence of $NaBH_4$ using green synthesized nanocomposite. Initially, on the surface of the catalyst, BH_4^- [$BH_4^- \rightarrow BH_3(OH)^-$] suggested that breakage in B–H bond and O–H bond, finally the reaction H–H bond formation. The 4-nitrophenolate on the surface of the catalyst accept the electron from BH_4^-. Transfer of electron was mainly depend on the adsorption and desorption of the synthesized catalyst surface. In the reduction of 4-NP, adsorption of the 4-nitrophenolate ions on the surface of nanocomposite (Ag/ZnO, Cu/ZnO and Ag-Cu/ZnO) and convert to 4-AP due to the interfacial electron transfer and leaves the surface of the nanocomposite to carry on a next catalytic cycle [45].

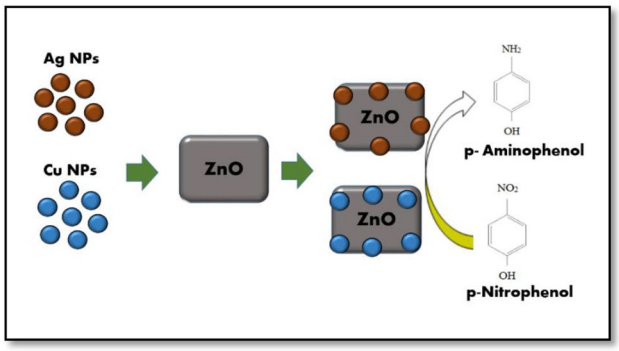

Scheme 1 Plausible mechanism of metal NPs ZnO nanocomposite on 4 NP reduction

3.2.4 Stability and Recyclability

The nanocomposite stability were evaluated by its reuse and recyclability experiments of CuNPs, Ag NPs, Cu@ZnO, and Ag@ZnO nanocomposite. The nanoparticles and nanocomposite of Cu and Ag were recovered by simple centrifugation after completion of the each catalytic reaction and reused in the next cycles. We conducted our experiment up to six cycles for both nanoparticles and nanocomposite. In heterogeneous catalytic activity of Cu and Ag NPs exhibited the conversion efficiency about 70% (Fig. 13a, b) and Cu/ZnO, and Ag/ZnO nanocomposite showed more 90% efficiency up to sixth cycle (Fig. 14a, b). The leaching of Cu and Ag NPs after completion of reaction were obtained by ICP-AES and it exhibited that 16 and 19% loss whereas lixiviating of metal content from the nanocomposite is about 7% loss in the Cu and nearly 9% loss in the Ag metals. The slight loss of catalyst might be during centrifugation and handling.

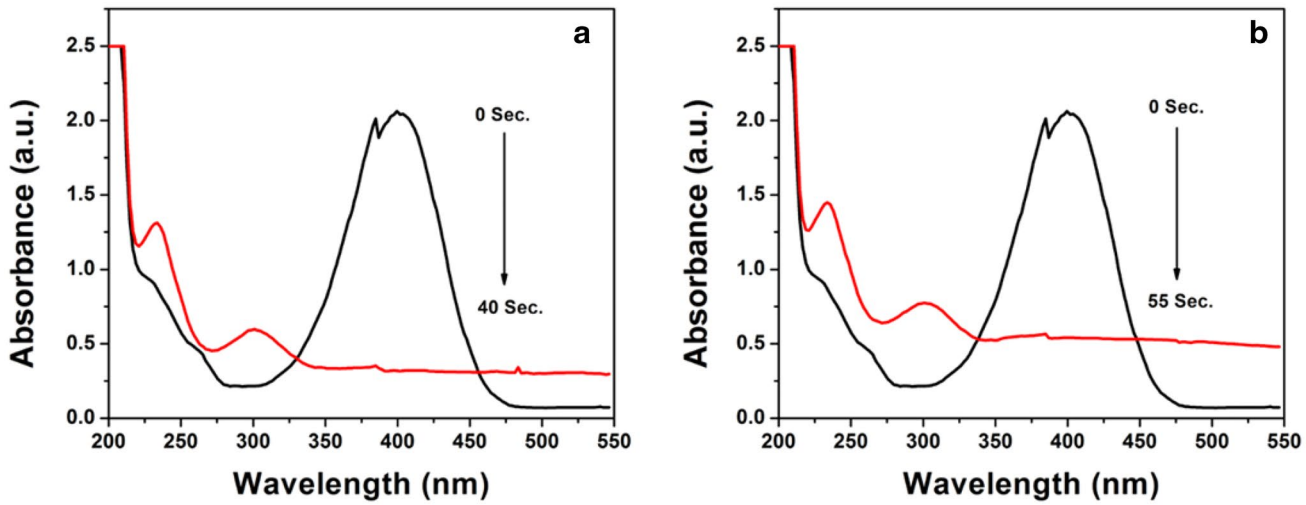

Fig. 12 UV–Vis spectra of heterogeneous reduction of 4-NP **a** Cu/ZnO and **b** Ag/ZnO nanocomposite

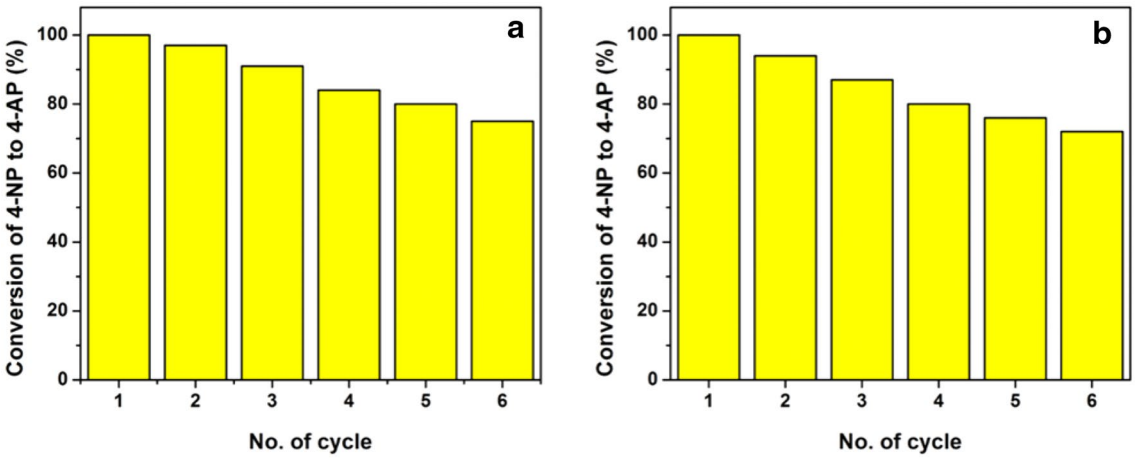

Fig. 13 Recyclability and reuse of heterogeneous catalyst **a** pure Cu and **b** pure Ag

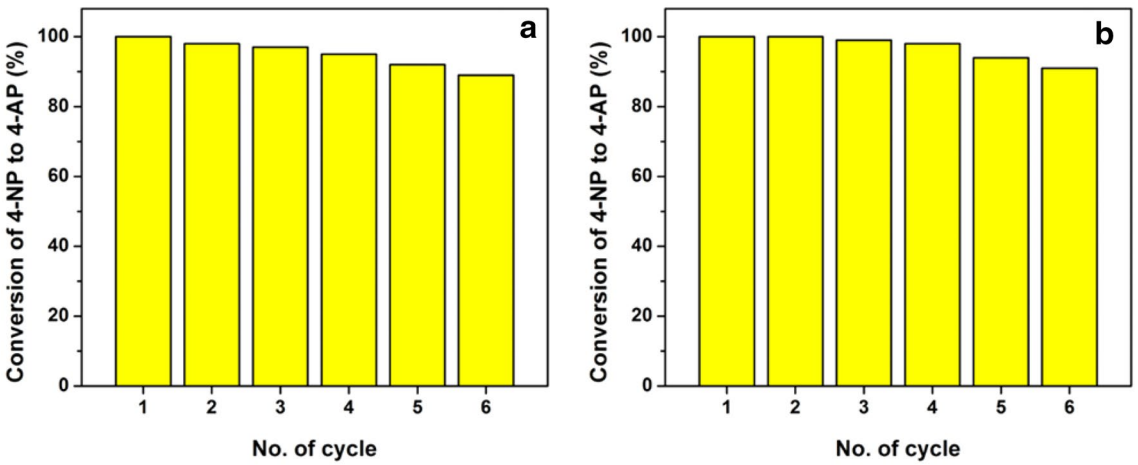

Fig. 14 Recyclability and reuse of heterogeneous catalyst **a** Cu/ZnO and **b** Ag/ZnO nanocomposite

4 Conclusion

The Cu, and Ag NPs and Cu@ZnO and Ag@ZnO nanocomposite were synthesized using aqueous bark extract of *A. elaeagnoidea*and characterized using UV–Vis Spectra, XRD, Raman spectra, TEM, SAED, EDAX, and FTIR. The Characterization reveals the formation of Cu and Ag nanoparticles with an average size 18 and 12 nm, immobilized over surface of ZnO. The synergetic effect between metal and porous material exhibited enhanced catalytic and recyclable activity than pure Cu and Ag NPs in both liquid and solid phase. As compared to Ag/ZnO, Cu/ZnO has exhibited eminently high heterogeneous catalytic activity in the reduction of p-NP. Finally, immobilization of metal nanoparticles over surface of porous material exhibited more stability and activity by easily dispersion of catalyst in reaction solutions. Ata same time reuse of the nanocatalyst by simple centrifugation, without significant loss activity. A facile, and cost effective route for synthesis of environmentally benign highly active catalyst.

Acknowledgements The authors are grateful to Pondicherry University for providing fellowship for the first two authors. The authors are acknowledge to STIC, Cochin and Central instrumentation facility, Pondicherry University for characterization analysis.

References

1. El-Sayed MA (2001) Some interesting properties of metals confined in time and nanometer space of different shapes. Acc Chem Res 34:257–264
2. Kelly KL, Coronado E, Zhao LL, Schatz GC (2003) The optical properties of metal nanoparticles: the influence of size, shape, and dielectric environment. J Phys Chem B 107:668–677

3. Suman TY, Rajasree SR, Jayaseelan C, Mary RR, Gayathri S, Aranganathan L, Remya RR (2016) GC–MS analysis of bioactive components and biosynthesis of silver nanoparticles using *Hybanthus enneaspermus* at room temperature evaluation of their stability and its larvicidal activity. Environ Sci Pollut Res 23:2705–2714
4. Murphy CJ, Gole AM, Hunyadi SE, Stone JW, Sisco PN, Alkilany A, Kinard BE, Hankins P (2008) Chemical sensing and imaging with metallic nanorods. Chem Commun 5:544–557
5. Saran S, Kamalraj G, Arunkumar P, Devipriya SP (2016) Pilot scale thin film plate reactors for the photocatalytic treatment of sugar refinery wastewater. Environ Sci Pollut Res 23:7730–17741
6. Padilla RH, Priecel P, Lin M, Lopez-Sanchez JA, Zhong Z (2017) A versatile sonication-assisted deposition–reduction method for preparing supported metal catalysts for catalytic applications. Ultrason Sonochem 35:631–639
7. Burda C, Chen X, Narayanan R, El-Sayed MA (2005) Chemistry and properties of nanocrystals of different shapes. Chem Rev 105:1025–1102
8. Bordbar M, Mortazavimanesh N (2016) Green synthesis of Pd/walnut shell nanocomposite using *Equisetum arvense* L. leaf extract and its application for the reduction of 4-nitrophenol and organic dyes in a very short time. Environ Sci Pollut Res 1–12
9. Crooks RM, Zhao M, Sun L, Chechik V, Yeung LK (2001) Dendrimer-encapsulated metal nanoparticles: synthesis, characterization, and applications to catalysis. Acc Chem Res 34:181–190
10. Wang MQ, Ye C, Bao SJ, Zhang Y, Xu MW, Li Z (2016) Bimetal–organic-frameworks-derived yolk–shell-structured porous Co_2P/ZnO@ PC/CNTs hybrids for highly sensitive non-enzymatic detection of superoxide anion released from living cells. Chem Commun 52:12442–12445
11. Sheng Q, Shen Y, Zhang J, Zheng J (2017) Ni doped Ag@ C core–shell nanomaterials and their application in electrochemical H_2O_2 sensing. Anal Methods 9:163–169
12. Goswami A, Rathi AK, Aparicio C, Tomanec O, Petr M, Pocklanova R, Gawande MB, Varma RS, Zboril R (2017) In situ generation of Pd–Pt core–shell nanoparticles on reduced graphene oxide (Pd@Pt/rGO) using microwaves: applications in dehalogenation reactions and reduction of olefins. ACS Appl Mater Interfaces 9:2815–2824
13. Cioffi N, Torsi L, Ditaranto N, Tantillo G, Ghibelli L, Sabbatini L, Bleve-Zacheo T, D'Alessio M, Zambonin PG, Traversa E (2005) Copper nanoparticle/polymer composites with antifungal and bacteriostatic properties. Chem Mater 17:5255–5262
14. Zhang Z, Zhang L, Wang S, Chen W, Lei Y (2001) A convenient route to polyacrylonitrile/silver nanoparticle composite by simultaneous polymerization–reduction approach. Polymer 42:8315–8318
15. Paul K, Gary AM (2014) Comprehensive organic synthesis, 2nd edn. Elsevier, New York
16. Udom I, Zhang Y, Ram MK, Stefanakos EK, Hepp AF, Elzein R, Schlaf R, Goswami DY (2014) A simple photolytic reactor employing Ag-doped ZnO nanowires for water purification. Thin Solid Films 564:258–263
17. Mori K, Miyawaki K, Yamashita H (2016) Ru and Ru–Ni nanoparticles on TiO_2 support as extremely active catalysts for hydrogen production from ammonia–borane. ACS Catal 6:3128–3135
18. Nasrollahzadeh M, Sajadi M (2016) Preparation of Pd/Fe_3O_4 nanoparticles by use of *Euphorbia stracheyi* Boiss root extract: a magnetically recoverable catalyst for one-pot reductive amination of aldehydes at room temperature. J Colloid Interface Sci 464:147–152
19. Nasrollahzadeh M, Sajadi SM, Rostami-Vartooni A, Alizadeh M, Bagherzadeh M (2016) Green synthesis of the Pd nanoparticles supported on reduced graphene oxide using barberry fruit extract and its application as a recyclable and heterogeneous catalyst for the reduction of nitroarenes. J Colloid Interface Sci 466:360–368
20. Pudukudy M, Yaakob Z, Mazuki MZ, Takriff MS, Jahaya SS (2017) One-pot sol–gel synthesis of MgO nanoparticles supported nickel and iron catalysts for undiluted methane decomposition into CO_x free hydrogen and nanocarbon. Appl Catal B 218:298–316
21. Ozgür U, Alivov YI, Liu C, Teke A, Reshchikov M, Doğan S, Avrutin VCSJ., Cho SJ, Morkoc H (2005) A comprehensive review of ZnO materials and devices. J Appl Phys 98:11–16
22. Zheng Y, Zheng L, Zhan Y, Lin X, Zheng Q, Wei K (2007) Ag/ZnO heterostructure nanocrystals: synthesis, characterization, and photocatalysis. Inorg Chem 46:6980–6986
23. Gao S, Jia X, Yang S, Li Z, Jiang K (2011) Hierarchical Ag/ZnO micro/nanostructure: green synthesis and enhanced photocatalytic performance. J Solid State Chem 184:764–769
24. Raja Rajeswari N, RamaLakshmi S, Muthuchelian K (2011) GC–MS analysis of bioactive components from the ethanolic leaf extract of *Canthium dicoccum* (Gaertn.) Teijsm & Binn. J Chem Pharm Res 3:792–798
25. Khare CP (2007) Indian medicinal plants: an illustrated dictionary. Springer Science Business Media, LLC, New York, p 393
26. Manjari G, Saran S, Rao AVB, Devipriya SP (2017) Phytochemical screening of *Aglaia elaeagnoidea* and their efficacy on antioxidant and antimicrobial growth. Int J Ayur Pharm Res 5:7–14
27. Ghosh S, Goudar VS, Padmalekha KG, Bhat SV, Indi SS, Vasan HN (2012) ZnO/Ag nanohybrid: synthesis, characterization, synergistic antibacterial activity and its mechanism. RSC Adv 2:930–940
28. Harish S, Archana J, Sabarinathan M, Navaneethan M, Nisha KD, Ponnusamy S, Muthamizhchelvan C, Ikeda H, Aswal DK, Hayakawa Y (2016) Controlled structural and compositional characteristic of visible light active ZnO/CuO photocatalyst for the degradation of organic pollutant. Appl Surf Sci 418:103–112
29. Ang W, Li X, Li S, Yan-Jun L, Wei-Wei L (2013) CuO nanoparticle modified ZnO nanorods with improved photocatalytic activity. Chin Phys Lett 30:046198–046202
30. Udom B, Pal PK (2011) Giri defect mediated magnetic interaction and high Tc ferromagnetism in Co doped ZnO nanoparticles. J Nanosci Nanotechnol 11:9167–9174
31. Lupan O, Chow L, Ono LK, Cuenya BR, Chai G, Khallaf H, Park S, Schulte A (2010) Synthesis and characterization of Ag-or Sb-doped ZnO nanorods by a facile hydrothermal route. J Phys Chem C 114:12401–12408
32. Kuriakose S, Satpati B, Mohapatra S (2014) Enhanced photocatalytic activity of Co doped ZnO nanodisks and nanorods prepared by a facile wet chemical method. Phys Chem Chem Phys 16(25):12741–12749
33. Soundarrajan P, Sankarasubramanian K, Sampath M, Logu T, Sethuraman K, Ramamurthi K (2015) Cu ions induced reorientation of crystallite in ZnO nano/micro rod arrays thin films. Phys E 71:56–63
34. Shankar SS, Ahmad A, Sastry M (2003) Geranium leaf assisted biosynthesis of silver nanoparticles. Biotech Prog 19:1627–1631
35. Manjari G, Saran S, Arun T, Rao AVB, Devipriya SP (2017) Catalytic and recyclability properties of phytogenic copper oxide nanoparticles derived from *Aglaia elaeagnoidea* flower extract. J Saudi Chem Soc 21:610–618
36. Saha S, Pal A, Kundu S, Basu S, Pal T (2009) Photochemical green synthesis of calcium-alginate-stabilized Ag and Au nanoparticles and their catalytic application to 4-nitrophenol reduction. Langmuir 26:2885–2893
37. Rode CV, Vaidya MJ, Chaudhari RV (1999) Synthesis of p-aminophenol by catalytic hydrogenation of nitrobenzene. Org Process Res Dev 3:465–470
38. Phan NT, Van Der Sluys M, Jones CW (2006) On the nature of the active species in palladium catalyzed Mizoroki–Heck and

Suzuki–Miyaura couplings–homogeneous or heterogeneous catalysis, a critical review. Adv Syn Cat 348:609–679
39. Gangula A, Podila R, Karanam L, Janardhana C, Rao AM (2011) Catalytic reduction of 4-nitrophenol using biogenic gold and silver nanoparticles derived from *Breynia rhamnoides*. Langmuir 27:15268–15274
40. Nasrollahzadeh M, Sajadi SM (2015) Green synthesis of copper nanoparticles using *Ginkgo biloba* L. leaf extract and their catalytic activity for the Huisgen [3 + 2] cycloaddition of azides and alkynes at room temperature. J Colloid Interface Sci 1:141–147
41. Choi Y, Bae HS, Seo E, Jang S, Park KH, Kim BS (2011) Hybrid gold nanoparticle-reduced graphene oxide nanosheets as active catalysts for highly efficient reduction of nitroarenes. J Mater Chem 21:15431–15436
42. Dhakshinamoorthy A, Asiri AM, Garcia H (2015) Metal–organic frameworks catalyzed C–C and C–heteroatom coupling reactions. Chem Soci Rev 44:1922–1947
43. Yao T, Zuo Q, Wang H, Wu J, Xin B, Cui F, Cui T (2015) A simple way to prepare Pd/Fe_3O_4/polypyrrole hollow capsules and their applications in catalysis. J Colloid Interface Sci 450:366–373
44. Momeni SS, Nasrollahzadeh M, Rustaiyan A (2016) Green synthesis of the Cu/ZnO nanoparticles mediated by *Euphorbia prolifera* leaf extract and investigation of their catalytic activity. J Colloid Interface Sci 472:173–179
45. Zhou Y, Fang C, Fang Y, Zhu F, Liu H, Ge H (2016) Hydrogen generation mechanism of BH^{4-} spontaneous hydrolysis: a sight from ab initio calculation. Int J Hydrog Energy 41:22668–22676